applied sciences

MDPI

Article

Analytical Study of Lateral Buckling of Pipelines with Initial Imperfection Based on Fixed-Fixed Beam Model

Songxian Wang [1], Lichen Li [1,*], Wenbing Wu [1,2,*], Tianwei Wang [1] and Hao Liu [1,2]

[1] Faculty of Engineering, Zhejiang Institute, China University of Geosciences, Wuhan 430074, China
[2] China Railway 16th Bureau Group No. 3 Engineering Co., Ltd., Huzhou 313000, China
* Correspondence: 20121003645@cug.edu.cn (L.L.); wuwb@cug.edu.cn (W.W.)

Abstract: The beam analysis model and the initial imperfection are predominant factors in analyzing the lateral buckling behavior of submarine pipelines under high temperature. However, the existing beam models do not consider the inhibition provided by the virtual anchor point of the pipeline. In this study, a fixed-fixed beam model is introduced to simulate the lateral buckling response of a submarine pipeline. This model considers the suppression tension provided by the virtual anchor point during the pipeline feeding-in process, which better reduces the buckling response phenomenon of the pipeline. Based on the assumption of rigid-plastic pipe-soil interaction, the analytical solution of the buckling development of pipeline under full-contact repetitive cosine imperfection is derived. The effectiveness of the fixed-fixed model is verified by comparing with the analytical solutions in other literature. The influence of the imperfection model, the temperature difference, and the soil resistance on the pipeline buckling is investigated. Finally, the size effect of the pipeline on the effective axial force development is discussed. The results show that the pipeline undergoes stress vibration under tensile force, and the frequency and density of the pipeline stress vibration increase with the increase of the initial defect amplitude. Increasing the diameter–thick ratio will significantly increase the bending amplitude and bending stress of the pipeline. Attention should be paid to the fatigue damage caused by continuous stress mutations during pipeline buckling, which could further lead to the structural destruction of the pipeline.

Keywords: submarine pipeline; lateral buckling; initial imperfection; fixed-fixed beam

Citation: Wang, S.; Li, L.; Wu, W.; Wang, T.; Liu, H. Analytical Study of Lateral Buckling of Pipelines with Initial Imperfection Based on Fixed-Fixed Beam Model. *Appl. Sci.* **2023**, *13*, 3227. https://doi.org/10.3390/app13053227

Academic Editor: Giuseppe Lacidogna

Received: 1 February 2023
Revised: 25 February 2023
Accepted: 28 February 2023
Published: 2 March 2023

1. Introduction

Submarine pipeline running at high temperature and high pressure will trigger global thermal expansion. When the axial pressure caused by the thermal expansion and the pressure increase is greater than the critical axial pressure of the pipeline, local buckling, fracture, fatigue, or excessive displacement of the pipeline would occur [1]. During the manufacturing or laying of submarine pipelines, imperfection would occur, which may develop into weak surfaces when the pipeline buckles. Therefore, it is necessary to study the lateral buckling behavior of submarine pipelines containing imperfection.

To date, considerable efforts have been made to improve the analytical understanding of the thermal buckling behavior of defective pipelines. Hobbs [2] first derived the analytical solution for both lateral and upheaval buckling of ideal submarine pipeline embedded on ideal rigid foundation, and deduced the corresponding critical axial force, buckling displacement amplitude, and bending moment based on the assumption of buckle mode. Taylor and Tran [3] conducted both theoretical analysis and experimental study on the axial buckling of pipelines under high temperature and high pressure. Three different initial geometric imperfections were investigated to obtain the critical flexion load of the submarine pipeline. In addition, Sriskandarajah et al. [4] analyzed the influence of the geometry of initial imperfection on the lateral buckling of submarine pipelines, and obtained the critical axial force of the lateral buckling of pipeline laying under different initial imperfection.

Zeng et al. [5]. derived the analytical solution of the critical buckling load considering the initial geometric imperfection size, imperfection waveform, and geometric instraightness (ω_{m0}/L_0) of the initial imperfection. Furthermore, Wang et al. [6] established an analytical solution for local buckling in unburied pipelines based on a nonlinear pipe-soil interaction model, and found that the snap-through required higher temperature differences between the pipes and the environment. Liu et al. [7] and Shi et al. [8] established an analytical solution for the high-order lateral overall buckling of the pipeline considering the single-arch symmetric initial imperfection and the double-arch antisymmetric initial imperfection.

For the analytical model of pipeline, pipeline has been modeled as moving beams placed on a rigid [9] or flexible [10] seabed. Hunt et al. [10] proposed the lateral buckling control equation of elastic rods with bending stiffness on buckling foundations, and since then, which provides the basis for most theoretical studies on the thermal buckling of submarine pipelines. Based on the Euler–Bernoulli beam theory, Kiani [11] and Wang et al. [12] studied the buckling of the beam under different types of thermal loads. Fu et al. [13] studied the thermal buckling of the pipe as a refined beam model, and analyzed the lateral shear deformation, volume fraction, and internal radius of the pipeline on the critical buckling. Mudhaffar et al. [14] analyzed the thermal buckling behavior of the pipeline at low temperature based on a viscoelastic plate model. Emam [15] discussed the formulation for the nonlinear buckling problem of buckling loads and posterior buckling states.

In recent years, scholars have found that when the pipeline releases the internal axial force through buckling deformation, a virtual anchor point (VAS) will form at the end of the slide segment [16,17]. The virtual anchor point divides the pipeline into multiple independent buckling short pipes. All existing analytical solutions for lateral buckling assume that the pipeline have infinite length, which indicates that the axial force at the end of the sliding segment is fully constrained. The axial force at the virtual anchor points between multiple buckles is less than the fully constrained axial force, and does not satisfy the basic assumption of the classical analytical solution. This problem belongs to the lateral buckling problem of the short pipe, and the classical analytical solution of the long tube is no longer applicable. In this study, a fixed-fixed beam model is introduced where the pipeline is regarded as a limited long beam, and both ends should keep a fixed distance during the buckling process. Compared to the existing studies, the fixed-fixed model additionally considered the tensile force generated in the pipe support section during the pipe buckling, which is suitable for the lateral buckling of the short pipes.

On the other hand, the finite element method (FEM) is also widely used in the study of lateral buckling behavior of submarine pipelines. Walker et al. [18] studied the influence of soil friction coefficient, material properties of the pipeline, and the maximum vertical strain of the virtual anchor spacing (VAS) on the global thermal buckling of the submarine pipeline. Based on the calibrated numerical simulation method, Haq et al. [19] studied the effect of external hydrostatic pressure, internal pressure, thermal expansion, and geometric instraightness (ω_{m0}/L_0) of the pipeline. Liang et al. [20] studied the lateral buckling of submarine pipelines laid on seabed pits and trenches. Zhang et al. [21] studied the effect of the initial imperfection on the critical axial force of the transverse buckling, and proposed a simple formula for the critical force calculation.

Both the initial imperfection and the beam analysis model have a great influence on the results of the buckling behavior analysis. In this study, a fixed-fixed beam model, considering the influence of initial imperfection, is introduced to study the lateral buckling problem of a pipeline with virtual anchor points. The analytical solution is first derived based on the full contact imperfection model and the fixed-fixed beam model. The analytical solution results are compared with numerical results from other scholars. Then the size effects of the short pipeline and the effects of the imperfection are discussed in detail, and the effect of the soil constraints on the lateral buckling of pipelines embedded on different seabed is studied.

2. Mathematical Model and Assumptions

Due to the incomplete structure of the pipeline and the initial imperfection, pipelines are more prone to lateral buckling with the decrease of critical temperature difference. As shown in Figure 1, when full-contact repeat imperfection is considered, the imperfection profile can be expressed as:

$$\omega_0(\mathrm{x}) = \frac{\omega_{\mathrm{m0}}}{2}\sin(\lambda_{\mathrm{e}}x)\ 0 \le x \le L_0 \tag{1}$$

where $\lambda_{\mathrm{e}} = \pi/L_0$; ω_{m0} is the amplitude of imperfection and L_0 is the half wavelength of imperfection.

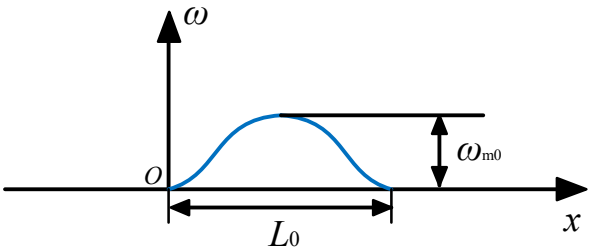

Figure 1. Modes of the initial imperfection.

For submarine pipelines, there is a temperature difference ΔT between the fluid flowing inside the pipe and the environment. If the pipe can expand, the axial compressive strain caused to thermal expansion will accumulate at the axial resistance between the pipe and the seabed. Therefore, within the online elastic response range, the axial compressive force P_0 corresponding to the axial strain should be written as:

$$P_0 = AE\alpha\Delta\mathrm{T} \tag{2}$$

where E is the elastic modulus, A is the cross-sectional area of the pipeline, α is the linear thermal expansion coefficient.

The lateral buckling behavior of the pipeline is simulated using the linear beam theory. The equation controlling the lateral imperfection of the beam is [22]:

$$EI\frac{d^4\omega}{dx^4} + P\frac{d^2\omega}{dx^2} = -F_A - P\frac{d^2\omega_0}{dx^2} \tag{3}$$

where P is the effective axial compression force at the center of the buckle, F_A is the axial soil resistance, ω is pipeline buckling amplitude.

In this study, the sea bed is assumed to be fully rigid. A new parameter λ can then be introduced as follows:

$$\lambda^2 = \frac{P}{EI} \tag{4}$$

The general solution of the equation can be written as:

$$\omega(x) = \mathrm{A}_1 + \mathrm{A}_2x + \mathrm{A}_3\cos\lambda x + \mathrm{A}_4\sin\lambda x - \frac{F_A}{2\lambda^2 EI}x^2 + \frac{\omega_{\mathrm{m0}}\lambda^2}{2(\lambda_{\mathrm{e}}^2 - \lambda^2)}\sin\lambda_{\mathrm{e}}x \tag{5}$$

The pipeline at the anchor point (x = 0) of the buckling amplitude is inextensible, unshearable. So, the lateral deflection and slope must be zero.

$$\begin{cases} \omega(0) = 0 \\ \frac{d\omega}{dx}(0) = 0 \end{cases} \tag{6}$$

At the other end of the pipeline, buckling amplitude, shearing force, and bending moment are zero at $x = L_S$.

$$\begin{cases} \omega(L_S) = 0 \\ \frac{d\omega}{dx}(L_S) = 0 \\ \frac{d^2\omega}{dx^2}(L_S) = 0 \end{cases} \tag{7}$$

Combining Equations (5)–(7), the solved equation coefficients are:

$$\begin{cases} A_1 = \frac{F_A}{\lambda^4 EI} \\ A_2 = -\frac{F_A L_S}{\lambda^2 EI(1-\lambda \cos \lambda L_S)} + \frac{\omega_{m0}\lambda^2\lambda_e(\lambda \cos \lambda L_S - \cos \lambda_e L_S)}{2(\lambda_e{}^2-\lambda^2)(1-\lambda \cos \lambda L_S)} \\ A_3 = -\frac{F_A}{\lambda^4 EI} \\ A_4 = -\frac{F_A L_S}{\lambda^3 EI(1-\lambda \cos \lambda L_S)} + \frac{\omega_{m0}\lambda\lambda_e(2\lambda \cos \lambda L_S - 1 - \cos \lambda_e L_S)}{2(\lambda_e{}^2-\lambda^2)(1-\lambda \cos \lambda L_S)} \end{cases} \tag{8}$$

The buckling part of the pipe is regarded as a separate short pipe and divided into three parts, namely the buckle section ($0 < x < L_0 + \Delta L$), the sliding section ($L_0 + \Delta L < x < L_S$), and the anchor section ($x > L_S$). As shown in Figure 2, the central part of the pipeline will move horizontally during lateral buckling. Then, when the pipeline enters the buckling section, the effective axial compression force of the pipe drops, pulling more pipes into the buckling.

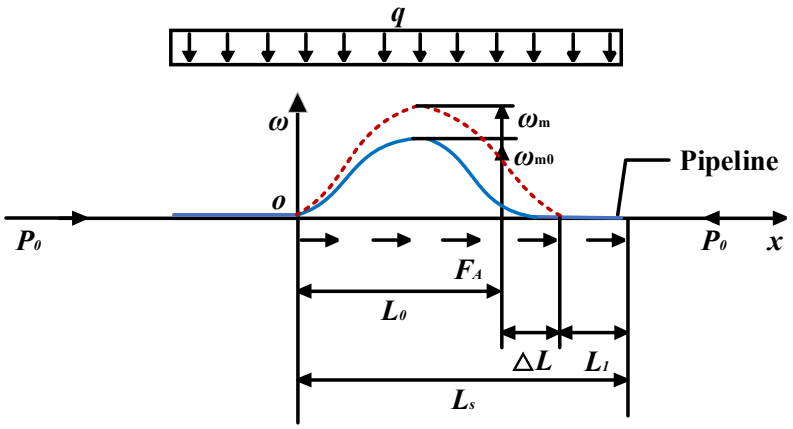

Figure 2. Configuration and loads distribution.

Based on the profile of axial compressive force shown in Figure 3, the distribution of axial compressive force $P(x)$ is written as:

$$P(x) = P - N + F_A x \ (0 \le x \le L_S) \tag{9}$$

where N is the tension force corresponding to the beam tension. The axial friction force can be expressed as:

$$F_A = \mu_A q \tag{10}$$

where μ_A is the axial friction coefficient between pipeline and seabed, and q is the submerged weight per unit length of the pipeline.

Combining Equations (1), (3) and (19), the axial force balance is obtained:

$$AE\alpha\Delta T = EI\lambda^2 - N + \mu_A q L_S \tag{11}$$

Burgreen [23] and McDonald [24] proposed a beam model considering the linear elastic isotropic response of beam under compressive axial force P_0. If the pipeline end remains fixed in space and the axial compression load exceeds the critical buckling load, lateral buckling of the pipeline occurs. During lateral buckling, the buckling area gradually

expands along the pipeline length, and the pipeline experiences planar feeding-in during lateral buckling. As shown in Figure 4, the effective compression load at the support of the pipeline reduces the tension generated along the buckling, reducing the initial axial compression load and thus reducing the support reaction [25].

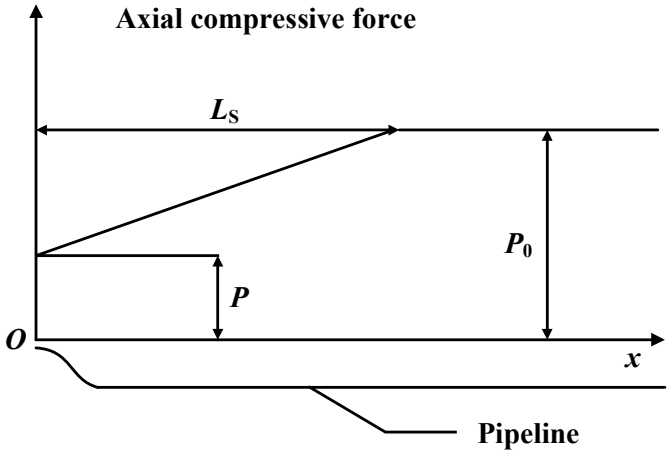

Figure 3. Axial compression distribution of pipe lateral buckling.

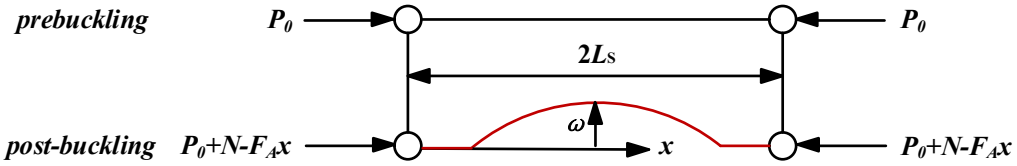

Figure 4. A Schematic of the bending deformation of the end fixed-fixed beam under the compression condition.

Assuming that the pipeline is a limited long beam, the bending of the beam is allowed while the two ends remain fixed. Based on this assumption, the pipeline buckling shows a midplane stretching phenomenon when the effective axial stress exceeds the buckling stress. In the range of second-order effects, the midplane stretch due to buckling is defined as the feeding-in segment length and can be expressed as:

$$L_1 = \frac{1}{2}\int_0^{L_S} \frac{d\omega}{dx} dx \tag{12}$$

Based on Equation (12), the corresponding tensile force N at the beam supports can be given by Hooke's law [25]:

$$N = \frac{EA}{L} L_1 \tag{13}$$

For the eigenvalue problem of beam vibration under temperature load, there is the following eigenvalue equation:

$$(P_0 + 4{\omega_L}^2) \sin k_1 \sin \lambda k_2 = 0 \tag{14}$$

where ω_L is the linear natural frequency and k_1 and k_2 are two constants given by:

$$\begin{cases} k_1 = \sqrt{\frac{1}{2}(P_0 + \sqrt{{P_0}^2 + 4{\omega_L}^2})} \\ k_2 = \sqrt{\frac{1}{2}(-P_0 + \sqrt{{P_0}^2 + 4{\omega_L}^2})} \end{cases} \tag{15}$$

Since ω_L must be positive, Equation (14) yields $k_1 = n\pi$ and the linear natural frequency of the first mode is given by:

$$\omega_{\mathrm{L}}{}^2 = \pi^2(\mathrm{AE}\alpha\Delta\mathrm{T} - \pi^2) \tag{16}$$

For the fixed-fixed beam, the linear natural frequency of the first mode can be obtained by solving the following transcendental equation:

$$2k_1k_2(\cos k_1 \cos \lambda k_2 - 1) + (k_1 - k_2)(k_1 + k_2) \sin k_1 \sin \lambda k_2 = 0 \tag{17}$$

Considering the bending stress distribution along the pipeline, the moment M along the bending pipeline is:

$$M = EI(\frac{d\omega^2}{d^2x} - \frac{d{\omega_0}^2}{d^2x}) \ (0 \le x \le L_S) \tag{18}$$

It is concluded that the corresponding bending stress σ_{m} along the bending pipe is:

$$\sigma_{\mathrm{m}} = \frac{MD}{2I} \tag{19}$$

where D is the pipeline external diameter.

The maximum axial compression stress σ_{m} along the pipeline is composed of the maximum bending stress σ_{Mm} and the axial compression stress σ_{P}:

$$\sigma_{\mathrm{m}} = \sigma_{\mathrm{p}} + |\sigma_{\mathrm{Mm}}| \tag{20}$$

The axial compression stress σ_{P} is:

$$\sigma_{\mathrm{p}} = \frac{P_0}{A} \tag{21}$$

The maximum bending stress σ_{Mm} is:

$$\sigma_{\mathrm{Mm}} = \frac{M_{\mathrm{m}}D}{2I} \tag{22}$$

3. Comparison

Based on the cantilever beam assumption [26] and the simplified fixed-fixed beam assumption [27], a fixed-fixed beam model is proposed to simulate the buckling response of short pipe. As shown in Figure 5, the analysis results are first compared with numerical results. The trend of the buckling distribution in Figure 5a is roughly the same as the distribution in the study of Lagrange [26] and Wang [27]. It can be seen that the maximum value of buckling (ω_{m}) is less than that in the study of Lagrange and Wang under the suppression of the buckling deformation. Meanwhile, the relationship between the effective axial force and the maximum value of the buckling is shown in Figure 5b. The effective axial force becomes larger as the maximum value of the buckling increases. But when the fixed-fixed beam model is considered, the posterior buckling behavior of the pipeline will be suppressed, so λ^2 decreases later when compared to the research of Lagrange. At the same time, due to the stress mutation of the pipeline under thermal vibration, the relationship between the effective axial force and the maximum value of the buckling in this study is not smooth. Therefore, the analytical model in this paper is reliable to simulate the thermal buckling of pipelines.

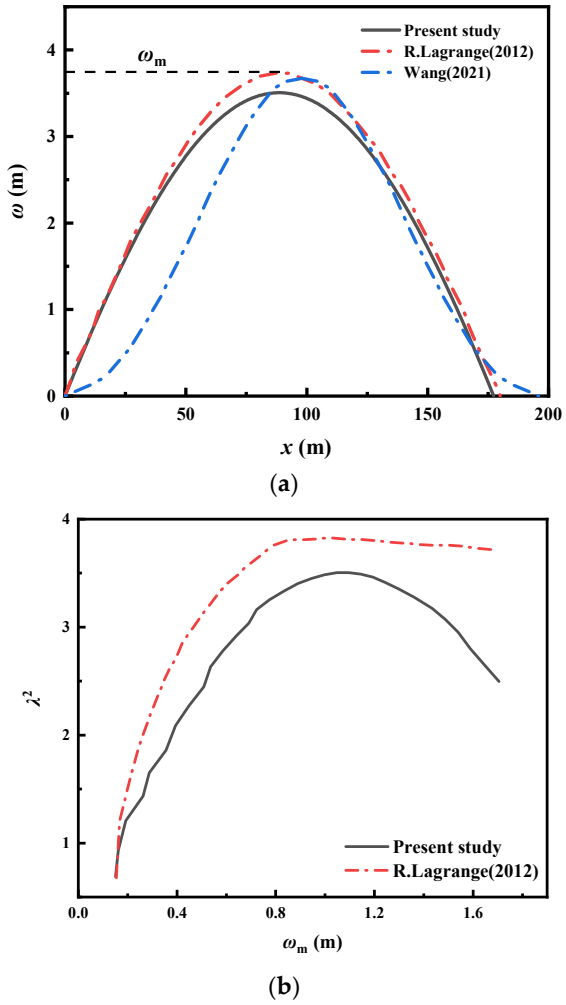

Figure 5. Comparison of buckling development of pipelines in different studies: (**a**) Comparison of the buckling distributions; (**b**) comparison of the buckling maximum to λ^2 [26,27].

4. Parametric Study

4.1. Initial Imperfection Effect

In this section, the effect of the amplitude of the initial imperfection ω_{m0} on the lateral buckling configuration and the typical lateral buckling behavior is analyzed. The pipeline parameters, pipeline properties, soil properties, and soil parameters are kept constant, as shown in Table 1.

Table 1. Parameters.

Parameter	Value	Unit
Elastic modulus E	206	GPa
External diameter D	0.65	m
Wall thickness t	0.0227	m
Steel density ρ	7850	kg/m^3
Moment of inertia I	1.509×10^{-3}	m^4
Coefficient of thermal expansion α	1.1×10^{-5}	$^\circ$C^{-1}
Axial friction coefficient μ_A	0.5	-

The buckling amplitude development and bending stress distribution of the pipeline with the variance of ω_{m0}/L_0 are shown in Figure 6. As the initial imperfection ratio increases, the global buckling amplitude of the pipeline also increases. From the buckling

deformation shown in Figure 6a, the initial imperfection ratio can greatly increase the buckling amplitude of the pipeline. The pipeline still deflects in the imperfection center as ω_{m0} increases. Therefore, the imperfection is the weak part of the pipeline, and stress concentration would occur at the imperfection.

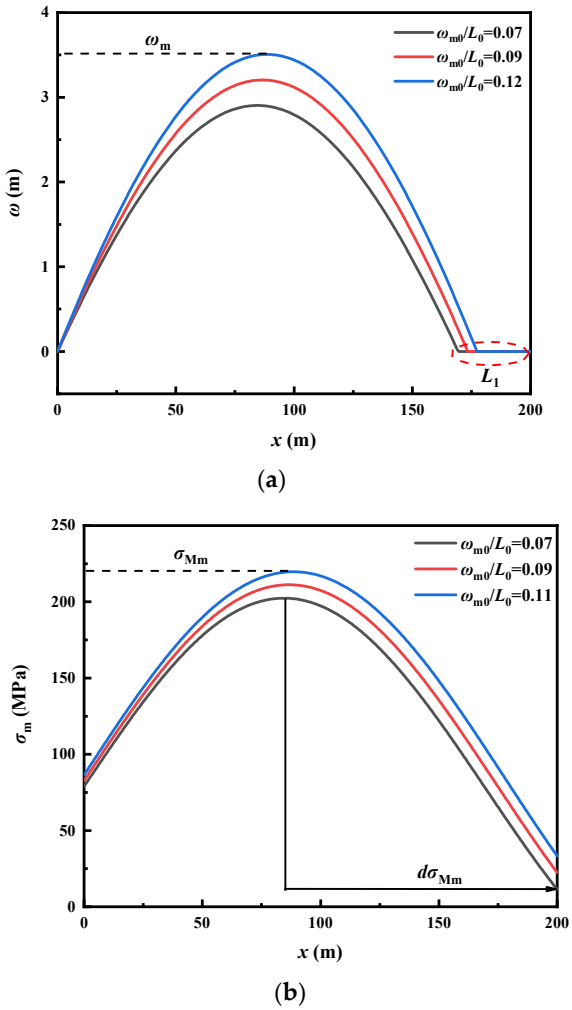

Figure 6. Effect of the initial imperfection on the buckling configuration: (**a**) Influence of ω_{m0} on deformation; (**b**) influence of ω_{m0} on bending stress.

In Figure 6b, the maximum bending stress is referred as σ_{Mm}. When the initial imperfection exists, the maximum axial compressive stress σ_{Mm} increases significantly with increasing initial imperfection ratio. With the increase of the initial imperfection, the maximum bending stress value moves in the positive direction of L_S. This is because as the imperfection locates closer to the center of the pipeline, the stress is more likely to be affected by the initial imperfection amplitude. Moreover, the feeding-in amplitude increases with the increase of the imperfection during the buckling of the fixed-end pipeline.

λ^2 is expressed as a dimensionless form of the effective axial compressive force, and the values of N and λ^2 can be obtained by solving the transcendental equations to obtain their relationship with the pipeline virtual anchor segment length L_S. During the lateral buckling of the pipeline, both λ^2 and the pull force N by the pipeline feeding-in will change with the initial imperfection ω_{m0}. They are related to the pipe virtual anchor segment length L_S. As can be seen from Figure 7a, as ω_{m0} increases, the N values will also decrease nonlinearly. This means that the bearing capacity of the pipeline decreases as the initial imperfection ratio increases. When the initial imperfection ratio remains unchanged, the bearing capacity increases from $L_S/L_0 = 3$ to $L_S/L_0 = 8$ and the corresponding tensile force

N decreases by 0.21 MN. The change in tension is more drastic, and its influence cannot be ignored.

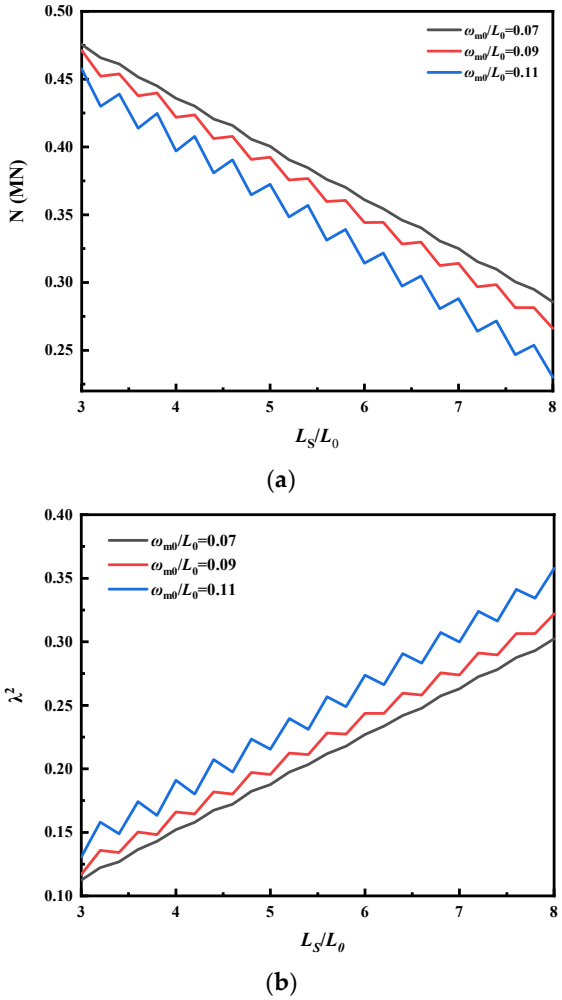

Figure 7. Changes in concentration forces during buckling under different ω_{m0} conditions: (**a**) tensile force N; (**b**) parameter λ^2.

It can be clearly seen that local stress vibration occurs with the decrease of L_S. And with increasing tension of the pipeline, the lateral buckling of the pipeline maintains the feed. When the pipeline is perfect, the local stress vibration is not obvious. However, when the initial imperfection is considered, the vibration becomes obvious. During continuous mutation, the pipeline has a fatigue effect. At the same time, as the influence of ω_{m0} increases, the vibrations effect becomes more obvious. As ω_{m0} increases, the frequency of the stress vibrations becomes denser and the buckling amplitude increases, which indicates stronger vibrations effect.

The rise of λ^2 implies the rise of the effective axial force, which leads to a greater probability of pipeline buckling. In Figure 7b, it can be seen that λ^2 increases with increasing initial imperfection ratio, thus increasing the possibility of lateral buckling of the pipeline. Similar to Figure 7a, the same local mutation also exists with the nonlinear growth of λ^2. It can be found that the imperfection amplitude ω_{m0} has a great influence on the thermal buckling behavior. It can be found that both the initial imperfection of the pipeline and the increasing amplitude of the imperfection will increase the risk of lateral buckling of the pipeline, and have an obvious impact on the thermal vibration of the pipeline.

4.2. Pipeline Design Size Effect

In this section, the effect of pipeline size on the lateral buckling of submarine pipelines is discussed. The pipeline size considered in this study includes the diameter–thick ratio and the virtual anchor segment length (VAS). The amplitude and the initial half-wavelength of the initial imperfection remain constant.

4.2.1. Virtual Anchor Segment (VAS) Length Effect

For pipelines with no installed triggers, the virtual anchor segment length L_S depends on the soil resistance. For pipelines that have triggers installed to control lateral buckle, the L_S is the space between the two triggers. The buckling deformation and amplitude of bending stress under different virtual anchor section lengths are shown in Figure 8a,b.

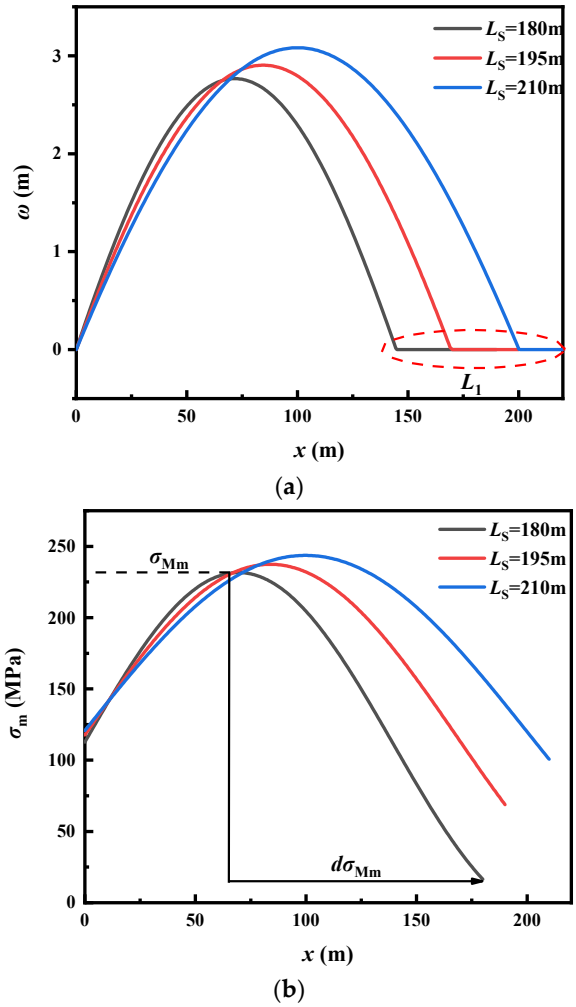

Figure 8. Effect of the virtual anchor segment length on the buckling configuration (ΔT = 70 °C): (**a**) deformed shapes; (**b**) bending stress.

When the length of the anchor section of the pipeline becomes larger, the amplitude of the buckle along the corresponding point of the pipeline increases, and the buckling extreme point will also move in the positive direction of the *x*-axis. This is followed by a decrease in the sliding segment distance when the trigger spacing is unchanged. As can be seen from Figure 8b, as the anchor segment lengths L_S of the pipeline keeps growing, the maximum bending stress increases, and the wavelength of the overall bending stress $d\sigma_{Mm1}$ becomes shorter. This leads to more drastic changes in the bending stress over a local area. At the same time, as the anchor segment lengths L_S becomes longer, the bending stress waveform moves toward the fixed point position. Therefore, the sensitivity of the

bending stress increases with the design length of the pipe, and the external bending stress is higher. This phenomenon means that under the fixed-fixed beam model, the probability of buckling instability is greater. Therefore, increasing the spacing of the triggers increases the risk of the pipes failure.

4.2.2. Diameter–Thick Ratio Effect

The effect of pipeline diameter–thick ratio on lateral buckling is analyzed at a constant trigger length (L_S = 200 m). As shown in Figure 9, the increase in the diameter–thick ratio leads to increasing bending stress, but the global distribution of bending stress remains unchanged. With the same wall thickness, the increase in pipeline external diameter would result in increasing liquid flow volume in the pipeline, as a result, the axial force and the bending stress of the pipeline increase. Since the effective axial force provided by the overall thermal expansion of the pipeline is evenly distributed along the pipeline, the increase in the flow volume does not change the distribution state of the axial force. At a constant temperature of $\Delta T = 70\ ^{\circ}C$ and a constant wall thickness of t = 30 mm, the external diameter D affects the maximum axial compressive stress, as shown in Figure 10. The maximum axial stress increases linearly with the pipeline diameter–thick ratio. As shown in Figure 11, as the feeding-in section length increases, the received effective inhibitory tensile stress increases, and the anchoring effect of the pipeline is more obvious. The growth rate of tensile stress increases with the diameter–thick ratio. Therefore, large diameter pipeline are more likely to fail compared to small diameter pipeline during lateral buckling.

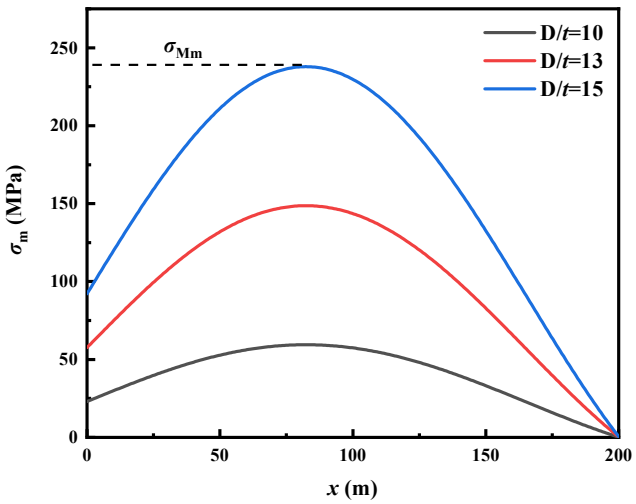

Figure 9. Effect of the external diameter D on bending stress.

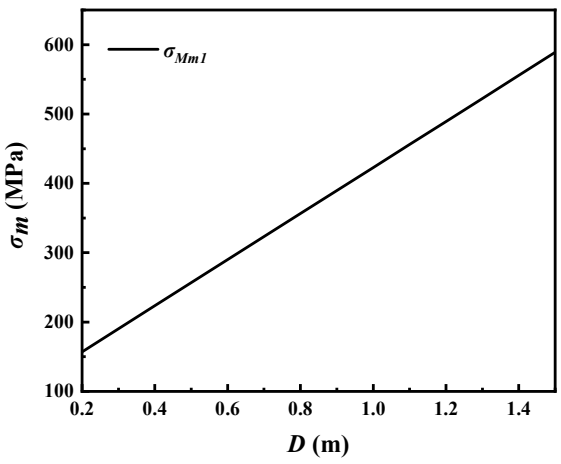

Figure 10. Effect of the external diameter D on the maximum axial force.

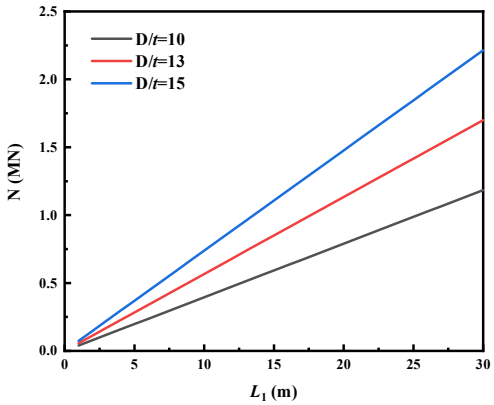

Figure 11. Changes in tensile force N during buckling under different diameter–thick ratio effect conditions (ΔT = 70 °C).

4.3. Temperature Effect

In this section, the influence of temperature rise load on the lateral buckling structure and typical lateral buckling behavior of submarine pipeline is discussed. The initial imperfection amplitude, initial half-wavelength, pipeline design parameters, pipeline appropriate relationships, soil characteristics, and those considered in Table 1 remain unchanged. The effects of temperature difference inside and outside the pipeline on the pipe buckling amplitude and bending stress distribution are shown in Figure 12a. In the constant imperfection condition, the buckling amplitude increases with the rise of pipeline temperature. The buckling state still shows a symmetric distribution at the imperfection. However, the feeding-in length decreases with increasing temperature, which reduces the suppression of the anchor point.

In Figure 12b, when the temperature difference increases, both the maximum axial compression stresses σ_{Mm} increase significantly. At the same time, an increase in the temperature difference causes the bending stress extreme point to move in the positive direction of L_{S}, and the value of $d\sigma_{\mathrm{Mm}}$ becomes smaller.

As can be seen from Figure 13, λ^2 increases linearly with the anchor point length as the temperature increases. At the same time, the effective axial force will grow faster with the increase of temperature, which risks the stability of the pipeline.

As shown in Figure 14, in the thermal vibration model, the vibration frequency of the pipeline increases with increasing temperature, and the thermal expansion force will cause the thermal vibration effect of the pipeline material. At the same time, the increase rate of the linear natural frequency becomes faster with the increase in the pipeline diameter–thick ratio.

4.4. Soil Resistance Effect

Soil resistance is a key factor affecting the lateral buckle shape of the pipeline. Previous studies showed that the high transverse resistance was beneficial for the lateral buckling stability, but would lead to increasing bending moment [28–31]. Figure 15 shows the lateral displacement and bending moment of the pipeline under different soil resistance coefficients μ_{A}. As shown in Figure 15a, with the increase of soil resistance, the lateral buckle near the middle part of the pipeline tends to accumulate, and the maximum buckling amplitude decreases. Moreover, the suppression of the deformation is more serious with increasing distance to the midpoint. As can be seen from Figure 15b, the increase in soil resistance will increase the distance between the extreme value and the anchor point while increasing the maximum value of the bending moment, and further inhibiting the deformation. This result is also in line with the actual engineering situation. As can be seen from Figure 16, an increase in soil resistance increases the effective axial force. With the absence of initial imperfection, the increase of soil resistance will also increase the stress mutation of the pipeline.

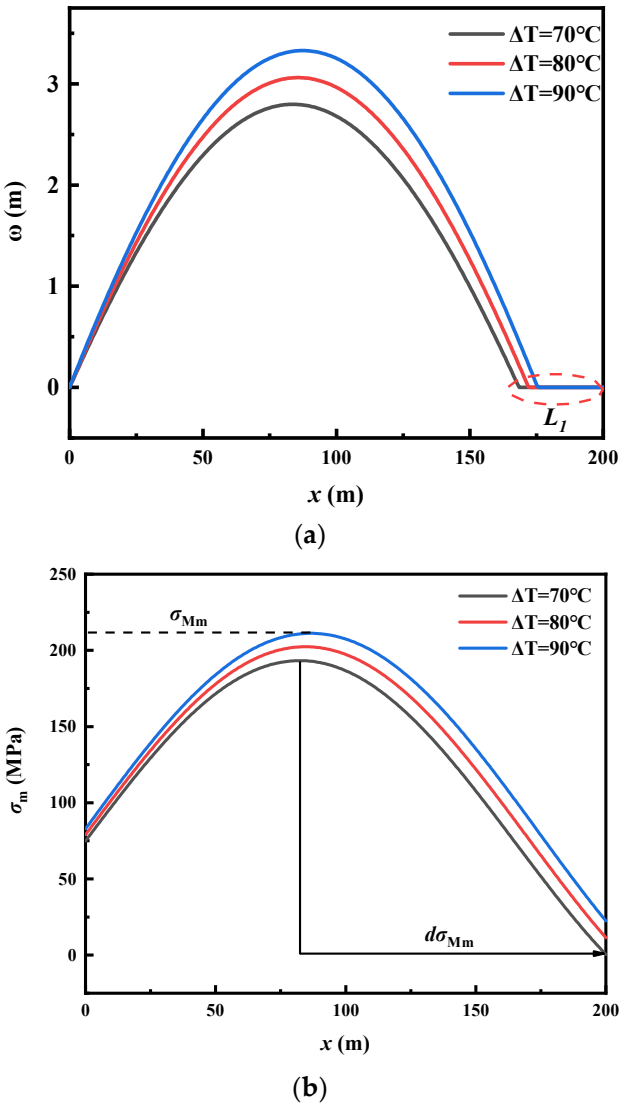

Figure 12. Effect of the temperature difference on the buckling configuration: (**a**) influence of ΔT on deformation; (**b**) influence of ΔT on bending stress.

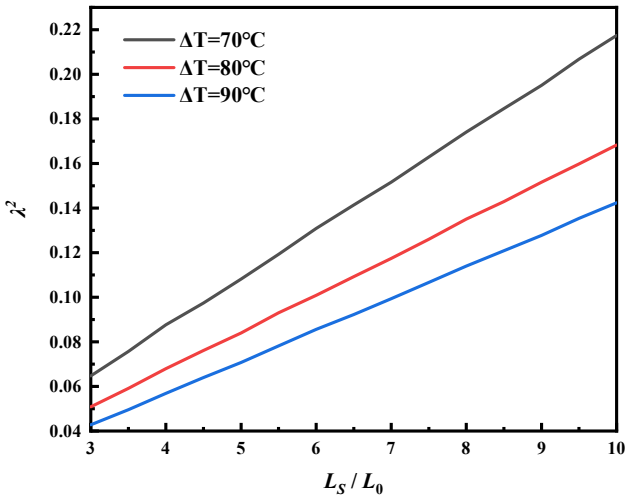

Figure 13. Changes in concentration forces during buckling under different ΔT conditions ($\omega_{m0} = 0$).

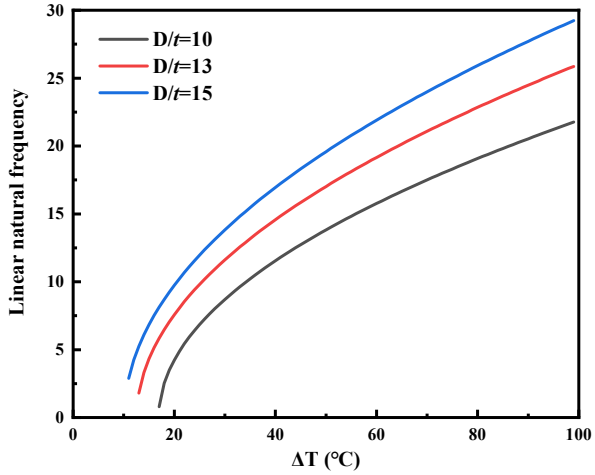

Figure 14. The linear natural frequency of pipeline varies with temperature difference under different diameter–thick ratio.

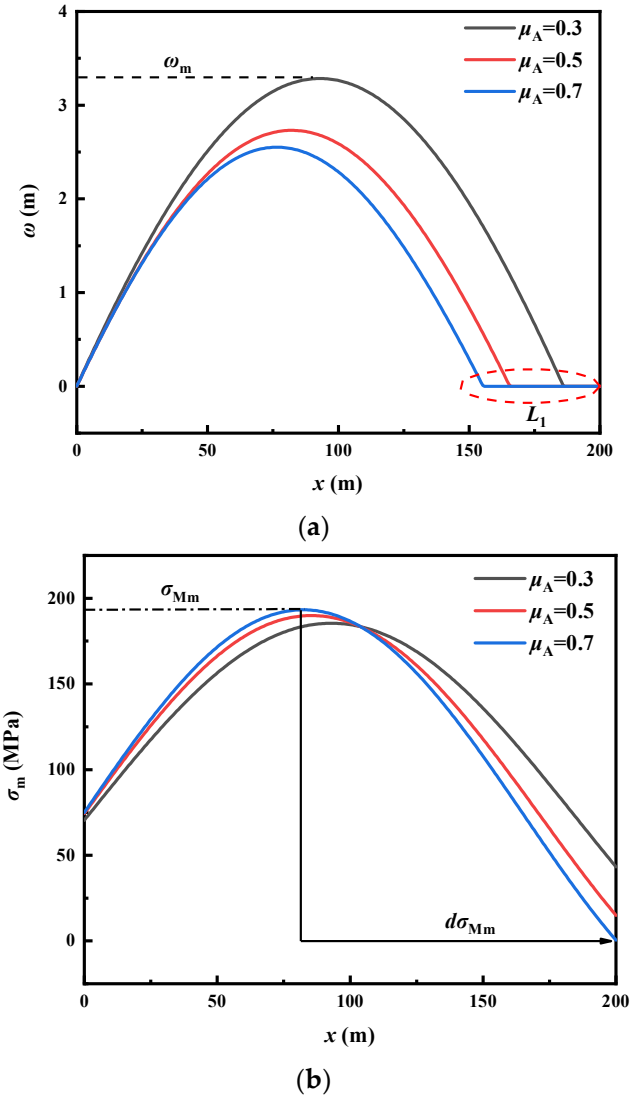

Figure 15. Effect of the solid resistance on the buckling configuration: (**a**) Influence of μ_A on deformation; (**b**) influence of μ_A on bending stress.

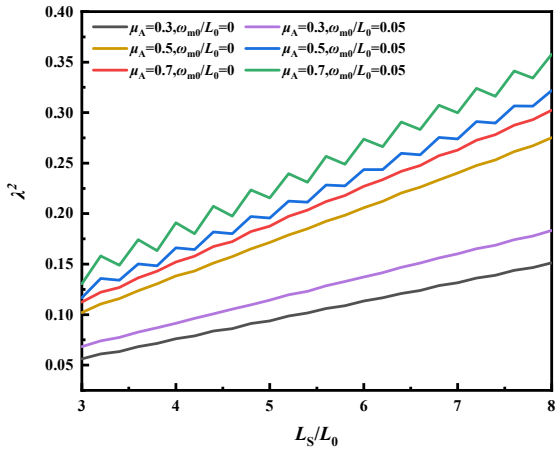

Figure 16. Change in parameter λ^2 during buckling under different solid resistance conditions.

5. Conclusions

An analytical solution is provided for the lateral buckling of the seabed pipeline based on the fixed-fixed ends beam model, considering the initial imperfection. The distribution of the external stress and displacement is determined by comparing the different extreme values of the axial compression stress and displacement amplitudes. The influence of the pipeline diameter–thick ratio effect on the buckling behavior is then analyzed. A detailed parametric analysis investigates the effects of temperature loading, imperfection amplitude, soil resistance on lateral buckling development and thermal vibration. The following conclusions can be drawn:

1. When the virtual anchor section divides the pipeline into multiple short sections, the thermal vibration phenomenon can be found based on the fixed-fixed beam model. The thermal vibration of the beam will cause the fatigue effect when the pipe bears the thermal load or the axial load, reducing the service life of the pipe. Therefore, when studying the lateral buckling problem of the pipeline, attention should be paid to the thermal vibration effect of the pipeline.
2. With increasing initial imperfection amplitude, the displacement amplitude and bending stress of the pipe increase linearly and the maximum bending stress position moves toward the position of the imperfection. At the same time, with increasing initial imperfection, the frequency and density of the pipeline stress vibration also increases, making the stress mutation effect more obvious. Attention should be paid to the fatigue disruption caused by continuous stress mutations in the pipeline during buckling.
3. Virtual anchor segment length (VAS) and diameter–thick ratio of the pipeline have an obvious influence on the behavior of lateral buckling. Increasing the diameter–thick ratio significantly increases the bending stress of the pipeline, and the anchoring effect of increasing the tensile stress on the pipeline. This is advantageous for the pipeline stability. When lateral buckling of the pipeline occurs, there is an obvious size effect. Therefore, in the pipeline design, the size effect of the pipeline must be considered.
4. With increasing temperature difference, the buckling amplitude and bending stress increase linearly. In addition, the maximum bending stress point moves in the positive direction of L_S, making the stress response at the pipe imperfection stronger. The corresponding tensile force also increases linearly with increasing temperature difference. Therefore, the pipeline running at high temperature is more likely to undergo lateral buckling at the initial imperfection.
5. As the soil resistance increases, the buckling amplitude decreases, and the bending stress increases accordingly. The maximum bending stress point moves toward the imperfection. With increasing soil resistance, pipe buckling is less likely to occur.

Therefore, it is prudent to prevent lateral buckling by increasing the effective friction coefficient, such as by digging trench lines.

Author Contributions: Conceptualization, S.W., L.L. and W.W.; methodology, S.W., W.W. and H.L.; software, S.W., T.W. and H.L.; validation, S.W., T.W. and H.L.; formal analysis, S.W., L.L. and H.L.; investigation, S.W., W.W. and H.L.; resources, L.L. and W.W.; data curation, S.W. and T.W.; writing—original draft preparation, S.W., L.L. and H.L.; writing—review and editing, W.W. and H.L.; supervision, L.L., W.W. and H.L. All authors have read and agreed to the published version of the manuscript.

Funding: This research was funded by the National Natural Science Foundation of China (Grant Nos. 52178371, 52168046, 52178321, 52108347), the Exploring Youth Project of Zhejiang Natural Science Foundation (LQ22E080010), the Outstanding Youth Project of Natural Science Foundation of Zhejiang Province (Grant No. LR21E080005), the China Postdoctoral Science Foundation Funded Project (Grant No. 2022M712964), the Research Project of Engineering Research Centre of Rock-Soil Drilling & Excavation and Protection, Ministry of Education (Grant No.202203), the Zhejiang Province's 2022 Key R&D Plan Project-'Lingyan' Project (2022C03151), the Science and Technology Project of Zhejiang Provincial Communication Department (202305-2), the Construction Research Founds of Department of Housing and Urban-Rural Development of Zhejiang Province (Grant No. 2021K256).

Institutional Review Board Statement: Not appliable.

Informed Consent Statement: Not appliable.

Data Availability Statement: All the data used in this research can be easily accessible by downloading the various documents appropriately cited in the paper.

Conflicts of Interest: The authors declare no conflict of interest.

References

1. DNVGL-RP-F110. Global buckling of submarine pipelines structural design due to high temperature/high pressure. *Oslo Det. Norske Veritas* **2018**.
2. Hobbs, R.E. In-service buckling of heated pipelines. *J. Transp. Eng.* **1984**, *110*, 175–189. [CrossRef]
3. Taylor, N.; Tran, V. Experimental and theoretical studies in subsea pipeline buckling. *Mar. Struct.* **1996**, *9*, 59–78. [CrossRef]
4. Sriskandarajah, T.; Dong, S.; Sribalachandran, S. Effect of initial imperfections on the lateral buckling of subsea pipelines. In Proceedings of the 1999 9th International Offshore and Polar Engineering Conference (ISOPE-99), Brest, France, 30 May–4 June 1999; pp. 168–175.
5. Zeng, X.G.; Duan, M.L.; Che, X.Y. Critical upheaval buckling forces of imperfect pipelines. *Appl. Ocean Res.* **2014**, *45*, 33–39. [CrossRef]
6. Wang, Z.K.; van der Heijden, G.H.M. Mode jumping in the lateral buckling of subsea pipelines. *Mar. Struct.* **2021**, *80*, 103077. [CrossRef]
7. Liu, R.; Wang, X.Y. Lateral global buckling high-order mode analysis of a submarine pipeline with imperfection. *Appl. Ocean Res.* **2018**, *73*, 107–126. [CrossRef]
8. Shi, R.; Wang, L.; Guo, Z.; Yuan, F. Upheaval buckling of a pipeline with prop imperfection on a plastic soft seabed. *Thin-Walled Struct.* **2013**, *65*, 1–6. [CrossRef]
9. Croll, J.G.A. A simplified model of upheaval thermal buckling of subsea pipelines. *Thin-Walled Struct.* **1997**, *29*, 59–78. [CrossRef]
10. Hunt, G.W.; Bolt, H.M.; Thompson, J.M.T. Structural localization phenomena and the dynamical phase-space analogy. *Proc. R. Soc. Lond. A Math. Phys. Sci.* **1989**, *425*, 175–189.
11. Kiani, Y.; Eslami, M.R. Thermal buckling analysis of functionally graded material beams. *Int. J. Mech. Mater. Des.* **2010**, *6*, 229–238. [CrossRef]
12. Wang, Z.K.; Tang, Y.G.; Soares, C.G. Analytical and numerical study on lateral buckling of imperfect subsea pipelines with nonlinear lateral pipe-soil interaction model. *Ocean Eng.* **2021**, *221*, 108495. [CrossRef]
13. Fu, Y.M.; Zhong, J.; Shao, X.F.; Chen, Y. Thermal postbuckling analysis of functionally graded tubes based on a refined beam model. *Int. J. Mech. Sci.* **2015**, *96–97*, 58–64. [CrossRef]
14. Mudhaffar, I.M.; Tounsi, A.; Chikh, A.; Al-Osta, M.A.; Al-Zahrani, M.M.; Al-Dulaijan, S.U. Hygro-thermo-mechanical bending behavior of advanced functionally graded ceramic metal plate resting on a viscoelastic foundation. *Structures* **2021**, *33*, 2177–2189. [CrossRef]
15. Emam, S.; Lacarbonara, W. A review on buckling and post-buckling of thin elastic beams. *Eur. J. Mech.* **2022**, *92*, 104449. [CrossRef]
16. Zhang, Y.P.; Wang, Z.Q.; El Naggar, M.H.; Wu, W.B.; Wang, L.X.; Jiang, G.S. Three-dimensional wave propagation in a solid pile during torsional low strain integrity test. *Int. J. Numer. Anal. Methods. Geomech.* **2022**, *46*, 2398–2411. [CrossRef]

17. Zhang, J.; Wang, Z.K.; Soares, C.G. Lateral buckling of subsea pipelines triggered by a sleeper with lateral constraint. *Ocean Eng.* **2021**, *234*, 109306. [CrossRef]
18. Walker, A.C.; Chee, K.Y.; Cooper, P. Particular aspects regarding the lateral buckling analysis of flowlines. In Proceedings of the ASME 2010 29th International Conference on Ocean, Offshore and Arctic Engineering, Shanghai, China, 6–11 June 2010; pp. 49–56.
19. Haq, M.M.; Kenny, S. Lateral buckling response of subsea HTHP pipelines using finite element methods. In Proceedings of the ASME 2013 32nd International Conference on Ocean. Offshore and Arctic Engineering, Nantes, France, 9–14 June 2013; pp. 1–8.
20. Liang, Z.; Lu, X.; Zhang, J. Thermal vertical buckling of surface-laid submarine pipelines on a sunken seabed. *Ocean Eng.* **2019**, *173*, 331–344. [CrossRef]
21. Zhang, X.; Duan, M. Prediction of the upheaval buckling critical force for imperfect submarine pipelines. *Ocean Eng.* **2015**, *109*, 330–343. [CrossRef]
22. Zhang, X.; Guedes, S.C.; An, C.L.; Duan, M. An unified formula for the critical force of lateral buckling of imperfect submarine pipelines. *Ocean Eng.* **2018**, *166*, 324–325. [CrossRef]
23. Burgreen, D. Free vibrations of a pin-ended column with constant distance between pin ends. *J. Appl. Mech.-T Asme.* **1951**, *18*, 135–139. [CrossRef]
24. McDonald, P.H. Nonlinear dynamic coupling in abeam vibration. *J. Appl. Mech.-T Asme.* **1955**, *22*, 573–578. [CrossRef]
25. Nayfeh, A.H.; Emam, S.A. Exact solutions and stability of the postbuckling configurations of beams. *Nonlinear Dynam.* **2008**, *54*, 395–408. [CrossRef]
26. Lagrange, R.; Averbuch, D. Solution methods for the growth of a repeating imperfection in the line of a strut on a nonlinear foundation. *Int. J. Mech. Sci.* **2012**, *63*, 48–58. [CrossRef]
27. Wang, Z.K.; Tang, Y.G.; Soares, C.G. Imperfection study on lateral thermal buckling of subsea pipeline triggered by a distributed buoyancy section. *Mar. Struct.* **2021**, *76*, 102916. [CrossRef]
28. Bruton, D.A.S.; White, D.J.; Carr, M.; Cheuk, J.C.Y. Pipe-soil interaction during lateral buckling and pipeline walking. *SAFEBUCK JIP.* **2008**, 2557–2576.
29. Wu, W.B.; Wang, Z.Q.; Zhang, Y.P.; El Naggar, M.H.; Wu, T.; Wen, M.J. Semi-analytical solution for negative skin friction development on deep foundations in coastal reclamation areas. *Int. J. Mech. Sci.* **2023**, *241*, 107981. [CrossRef]
30. Zhang, Y.P.; Di, T.Y.; El Naggar, M.H.; Wu, W.B.; Liu, H.; Jiang, G.S. Modified Rayleigh-Love rod model for 3D dynamic analysis of large-diameter thin-walled pipe pile embedded in multilayered soils. *Comput. Geotech.* **2022**, *149*, 104853. [CrossRef]
31. Wu, W.B.; Zhang, Y.P. A review of pile foundations in viscoelastic medium: Dynamic analysis and wave propagation modeling. *Energies* **2022**, *15*, 9432. [CrossRef]